A CFD-Based Numerical Evaluation, Assessment and Optimization of Conjugate Heat Transfer for Aerodynamic Cooling of a Wheel-Hub-Motors in Micro-Mobility Vehicles

Mambazhasseri Divakaran, A., Gkanas, E., Shepherd, S., Jewkes, J. & Abo-Serie, E

DOI 10.4271/2023-01-0760
ISSN 0148-7191
ESSN 0096-5170

Publisher: SAE International

A CFD-Based Numerical Evaluation, Assessment and Optimization of Conjugate Heat Transfer for Aerodynamic Cooling of a Wheel-Hub-Motors in Micro-Mobility Vehicles

Author, co-author (Do NOT enter this information. It will be pulled from participant tab in MyTechZone)

Affiliation (Do NOT enter this information. It will be pulled from participant tab in MyTechZone)

Abstract

Micro-mobility vehicles such as electric scooters and bikes are increasingly used for urban transportation; their designs usually trade off performance and range. Addressing thermal and cooling issues in such vehicles could enhance performance, reliability, life, and range. Limited packaging space within the wheels precludes the use of complex cooling systems that would also increase the cost and complexity of these mass-produced wheel motors. The present study begins by evaluating the external aerodynamics of the scooter to characterise the airflow conditions near the rotating wheel; then, a steady-state conjugate heat transfer model of a commercially available wheel hub motor (500W) is created using commercial computational fluid dynamics (CFD) software, StarCCM+. The CAD model of the motor used for this analysis has an external rotor permanent magnet (PM) brushless DC topology. Both internal and external fluid domains are considered to evaluate the combined flow dynamics and conjugate heat transfer from the windings (heat source) to the ambient air. At the maximum speed (482rpm) of the motor, for a total power loss of 180W (η=64%), a maximum temperature of 295°C is observed in the windings. Evaluating the thermal path shows that approximately 58.1% of the total heat generated in the winding is dissipated radially via convection through the air gap, and only 3.66% through the shaft via conduction. The thermal resistance for the shaft is in the range of 22-60 K/W and the rotor components is in the range of 0-2 K/W for the operational speed range of 0-1000rpm. Taguchi's Design of Experiment (DOE) with Design manager study has been conducted to optimize the performance of design parameters (Fins and air-vents/*holes*) in cooling the motor. Air vents and external fins on rotor–lid (rotor *cover*) has a greater effect on cooling the motor than other design parameters.

Introduction

Micro-mobility vehicles are arguably the future of urban transport as congested cities and towns become more common sights across the UK, and the wider world [1], [2]. During the period 2008/9 to 2014/15 the transport for London data indicates that the delay at traffic across the London city has increased by 20%. This consequently affect the economy, with an estimated £6.9 billion of productive working hours lost annually [2]. In addressing global economic and environmental impact, micro-mobility vehicles are considered as the sustainable travel mode with low economic and environmental impact and are the fastest growing convenient and affordable city transportation means [3], [4]. Accordingly, many cities across Europe and the US have introduced an e-scooter rental scheme for public use. Since 2020, UK government legislation has been amended to permit the rental of e-scooters for public use, the maximum speed and power being capped at 15mph and 500W, respectively [5], [6]. Nonetheless, personal lightweight electric vehicles are gaining popularity for urban transportation across the globe, and such vehicles are lightweight modes of transport for loads of less than 500kg at 25kmph speeds [7], [8]. The design of such vehicles usually trades off range against performance. Limited power and speed do not require a complex thermal management system, however, simple and efficient aerodynamic cooling can improve performance and range. In this research work, we focus in particular upon e-scooters.

The efficiency, stability, and lifespan of the traction motors used in electric vehicles can all be increased by the introduction of an effective heat management approach that will be able to remove heat efficiently from the powertrain system. Brushless DC wheel hub motors with permanent magnets (PM) have several benefits, such as increased efficiency and power density, a more straightforward transmission link, greater power output control and more interior space [9]. However, a major challenge is the effective cooling, as it is limited by the confined space [9]. Numerous publications can be found on various cooling methods used in electrical machines, such as winding liquid cooling, stator liquid cooling, shaft cooling and combined cooling with Phase change material and heat pipes [10]–[16]. These advanced cooling methods are not suitable for small outrunner motors such as PM brushless DC wheel hub motors (PMBLDC). Outrunner motor construction and application limits the use of complex cooling methods due to the restricted packaging space, so such motors mainly rely upon aerodynamic cooling [17]. The wheel hub motor cooling strategies are mostly focused on ensuring adequate heat dissipation from the electric coils to the ambient air by developing low thermal resistance paths. Thus, the main target is to reduce the temperature of the delicate parts, such as the windings, PMs and the bearings [18].

In the case of the PMBLDC hub motors, thermal analysis is necessary as almost all the thermal losses are produced in the stator windings. In addition, the structure limits the possible conductive path for the heat dissipation to the ambient only through the shaft. In this case, convection plays a significant role in dissipating the stator winding

losses as opposed to an internal rotor arrangement where the losses are dispersed by conduction [19], [20].

The hub motor can be on the front wheel or can be on the rear wheel of the e-scooters, both have their own advantages and disadvantages based on aerodynamics perspective, starting torque and transportation convenience. In this case, the heat transfer by convection dominates, whereas heat transfer via conduction limits the heat transfer only through the shaft. Heat accumulation within the motor may damage the windings, demagnetize the PMs and negatively affect the life and performance of the system [2],[10].

The UK government legally limit the maximum speed to 15mph and maximum power 500W for electric scooters to use in public [2]. Assuming this as the average speed and power limit across most of the countries in the world, throughout this study, the maximum speed and power is limited to 20kmph (12.4mph), which is 482rpm wheel speed and 500W motor power. Firstly, a CFD based study has been performed for external aerodynamics. In addition, the case of an extra passenger on a scooter has been considered, to allow the understanding of the fluid flowing in the wake region. Secondly, a3D CAD model of the motor was designed like the topology of a commercially available wheel-hub radial flux PM brushless DC machine *(48V, 3-phase, 500W)*, the wheel hub motor is analyzed for heat transfer path and interface thermal resistance considering both the external and internal fluid flow dynamics simultaneously. Designed commercial wheel-hub-motor was investigated for a conjugate heat transfer analysis with steady-state power loss of 180W in the windings. Finally, various design parameters such as internal and external extended surfaces (fins) and air vents/air channels on the rotor surface have been introduced and studied. Their performance was evaluated, to identify the optimum design parameters, with the highest effect in motor cooling. The optimized design parameter can be further optimized with ad-joint shape optimization to further enhance the heat transfer. Based on this a dynamic thermal model can be built to investigate further the dynamic performance with the optimized cooling approach.

The CFD based aerodynamic analysis of the scooter and wheel hub motor is carried out to investigate:

- The external fluid flow dynamics on the scooter with a passenger standing on it.
- The conjugate heat transfer from the windings to external ambient air considering both the internal and external fluid dynamics to determine the thermal path and thermal resistances.
- Taguchi's Design of Experiment (DOE) model with design manager study in StarCCM+ to optimise and identify the most effective design parameters required to maximise heat transfer and minimise winding temperature.
- To modify the most effective design parameters to further improve the heat transfer from windings to ambient air.

To propose a new cooling approach for ad-joint shape optimisation for further research study

Methodology - Computational Fluid Dynamics Analysis

In general, wheel hub motors mainly rely up on aerodynamic cooling. So understanding the external fluid flow is relevant in designing or modifying a rear wheel hub motor for improving aerodynamic cooling. So, here an external isothermal aerodynamics simulation analysis of a scooter with a passenger standing on it has been carried out before conducting a conjugate heat transfer analysis for the wheel hub motor. In this study, the wheel hub motor is located at the rear side of the scooter.

External Aerodynamics – Scooter with passenger standing on it

The external aerodynamics was carried out to identify the airflow distribution around the rear rotating wheel. In order to simulate the external aerodynamics of a scooter with a passenger standing on it, firstly, a 3D CAD geometry of the scooter and the passenger is imported. The scooter was located on a 3D virtual wind tunnel that includes the fluid domain. Steady incompressible airflow conditions are assumed with an isothermal condition. The outer four boundaries are set as slip walls. The flow is admitted to the fluid domain via the inlet velocity boundary and exit from the pressure outlet boundary as shown in Figure 1(a) Trimmed cell prism layer meshing is used for meshing the whole simulation domain, to avoid invalid meshing and for better solution convergence. Wheel patches have been introduced to both wheels of the scooter to avoid numerical error with invalid mesh. The simulation domain has been discretized to 4.75 million cells with more number of cells near wall boundaries of the scooter to improve the accuracy of the flow simulation. Such near wall refinement is critical in determining the wall forces, flow separations and heat transfer. Figure 1(b) shows the trimmed prism layer mesh distribution with finer mesh near the wall. The Spalart-Allmaras (S-A) turbulence model has been selected is widely used and has proven and numerically well behaved in most of the external aerodynamic fluid flow analysis [22]. Even though, S-A model is one equation model, it has been extensively validated for external flows and provides good agreement with experimental results particularly in aerospace applications in comparison to the two equation model such as k-epsilon and k-omega which performed relatively poorly in aerodynamic flows [23].

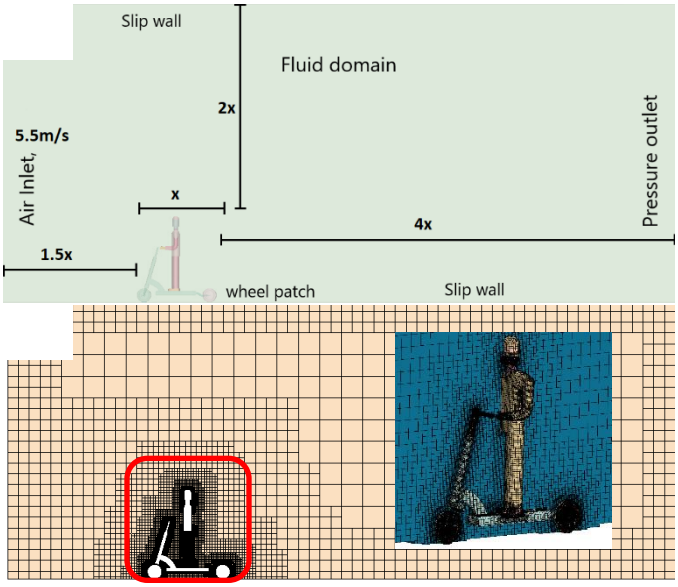

Figure 1. Shows the meshing and simulation domain with boundary conditions (a) fluid domain with boundary conditions (b) trimmed cell prism layer meshing

It is also set to identify the airflow velocity that can pass through a set of circumferential holes/air-vents located on the rotor, as shown in Figure 2(a-b). As the airflow depends on the pressure drop across the holes which in turn depends on external flow distribution, it was necessary to carry out an external aerodynamics analysis.

With this external aerodynamics simulation analysis, it is possible to identify the velocity distribution close to the wheel and the expected heat transfer coefficient. This evaluation also helps to introduce possible design modification to enhance the connective heat transfer from the rotating wheel. Additionally, another simulation analysis has been carried out with geometric modifications such as air holes/vents and fins on to the rotor surface.

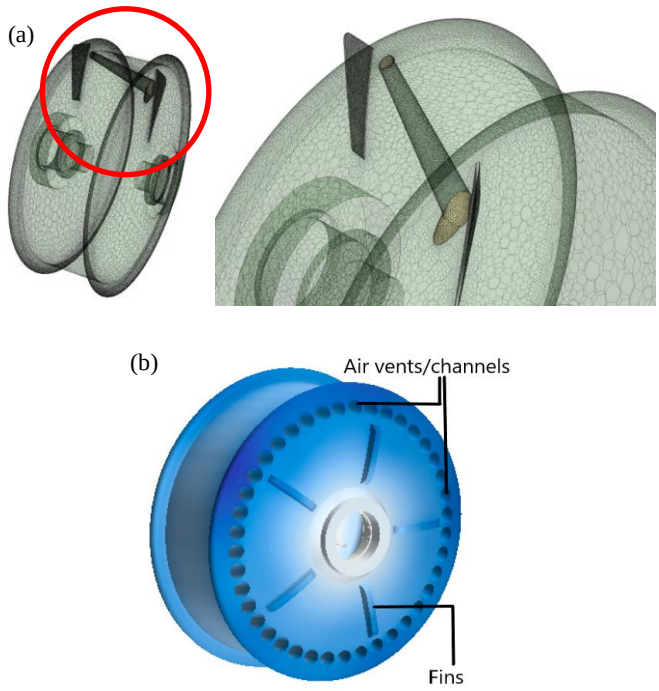

Figure 2. Shows the circumferential hole/air-vents and fins on the surface of the rotor for increasing the local velocity by generating pressure drop.

3D motor CAD design and CFD Simulation for conjugate heat transfer

In the conjugate heat transfer analysis the rear wheel motor has been analysed separately, a 3D CAD geometry of the wheel-hub motor has been re-drawn in Solidworks to remove the small holes and features that may affect the simulation before importing into STARCCM+. The motor model includes all of the major components, including the rotor, permanent magnets (PMs), sleeve, shaft, bearings, stator, and windings. Figure 3(a) presents the detailed 3D CAD design of the wheel hub motor. Table 1 lists out the thermal properties of the motor components used to set up the simulation. The computational simulation domain consists of the fluid domains and the solid domains. The rotating region, the internal fluid and the external fluid region constitute the fluid domains and the solid region consists of rotor, stator, sleeve, PMs, shaft, windings, and bearings. Figure 3(b) shows the simulation domain with the boundary conditions. The gray colored region is the solid region in the simulation domain.

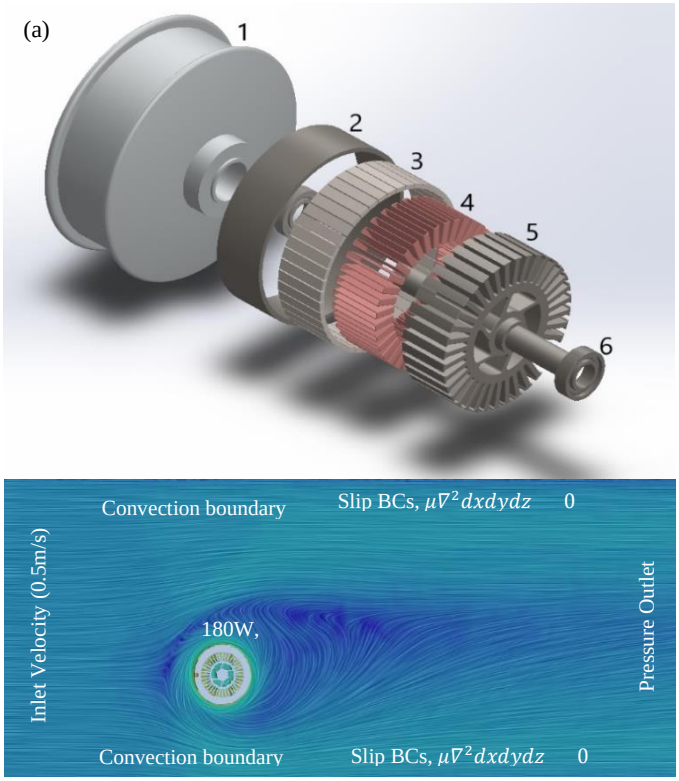

Figure 3. (a) Shows the exploded view of the 3D CAD design of wheel-hub-motor. 1-Rotor, 2-Sleeve, 3-Permanent Magnet, 4-Copper windings, 5-Stator and shaft, 6- Bearings. (b) Shows the simulation domain and boundary conditions applied in conjugate heat transfer analysis of the motor.

Both the external and internal fluid flow are solved together with the solid domain using the energy to evaluate the conjugate heat transfer. This coupled multi-fluid and solid simulation can predict all of the thermal paths and thermal resistances in the motor. Further, this serves as a guideline to introduce the aerodynamic design modifications or design parameters on the rotor or stator surfaces to enhance the heat transfer by reducing the thermal resistance. The external flow simulation is analysed to determine the heat transfer coefficient on the external surface of the rotor and internal flow to analyse the effect of narrow air-gap fluid flow dynamics in convective heat transfer. In this simulation, the Realisable two-layer k-epsilon turbulence model has been selected.

An in-place conjugate heat transfer contact mode interfaces with zero thermal resistance was set for the solid-solid and solid-fluid interfaces. The fluid enters the simulation domain with an inlet velocity of 0.5m/s at 20°C and exit through the pressure outlet boundary and other walls of simulation domain is set to slip convection boundaries (20°C, 20W/m^{2}K). The inlet velocity value is very small (0.5m/s) compared to the external aerodynamic inlet velocity (5m/s) condition because the simulation is carried out for the worst scenario *(assuming blockage in the fluid path to the rear wheel due to the presence of any kind of components)* analysis, high speed, and low available air velocity on wheels (*less than the value derived from the external aerodynamics*). The rotational reference frame is used to generate the rotational effect

of the rotor and reference frames are used to generate stationary boundaries and interfaces (ω =0), hence velocity gradient is ensured at the relevant boundaries. The rotating fluid region is set with a rotational reference frame of 482 rpm, which is equal to a scooter speed of 18kmph. For the multi-part solid region, energy source option is set to total heat source for windings. A constant heat load of 180W is set for the windings as the total power loss in the motor. At this power loss, motor efficiency is assumed to be 64% based on calculations available in literatures for a scooter motion [25], [26]. From these literatures, a scooter moving forward must overcome the aerodynamic drag, rolling friction and gradient force. Here in this study, a scooter and a passenger weighing 100kg in total is assumed moving on an uphill having a gradient greater than 3° at a constant speed of 18kmph could result in 180W of winding heat generation.

Table 1. Thermal properties of the BLDC motor components used for simulation analysis [24].

Material	Motor Components	Density (kg/m^3)	Specific heat capacity (J/kg°C)	Thermal conductivity (W/m°C)
Aluminum (alloy 195 Cast)	Rotor	2790	833	168
Laminated core pack	Stator	7800	460	28
Copper	windings	8954	400	386
Permanent Magnet	Magnets	7400	420	9
Steel	Sleeve, shaft	7800	460	30

Table 2. Technical specification of the motor

Specifications	
Power	500W
Voltage	36V, 3-Phase
Number of slots	36
Number of poles	18
Stator diameters	113mm
Rotor diameters	169mm
Wheel diameter	230mm
Stack length	37mm
Air gap length	0.5mm
Sleeve size	3.5x37mm

Conformal polyhedral with prism layer meshing is generated for both internal and external fluid flow simulation on the motor, which resulted in total of 34.6 million cells. Figure 4 presents the mesh independent or mesh convergence study and meshing of the simulation domain. For convergence and accurate flow simulation prism layers are used at the fluid sloid boundaries which is relevant to determine the wall forces and heat transfer across boundaries.

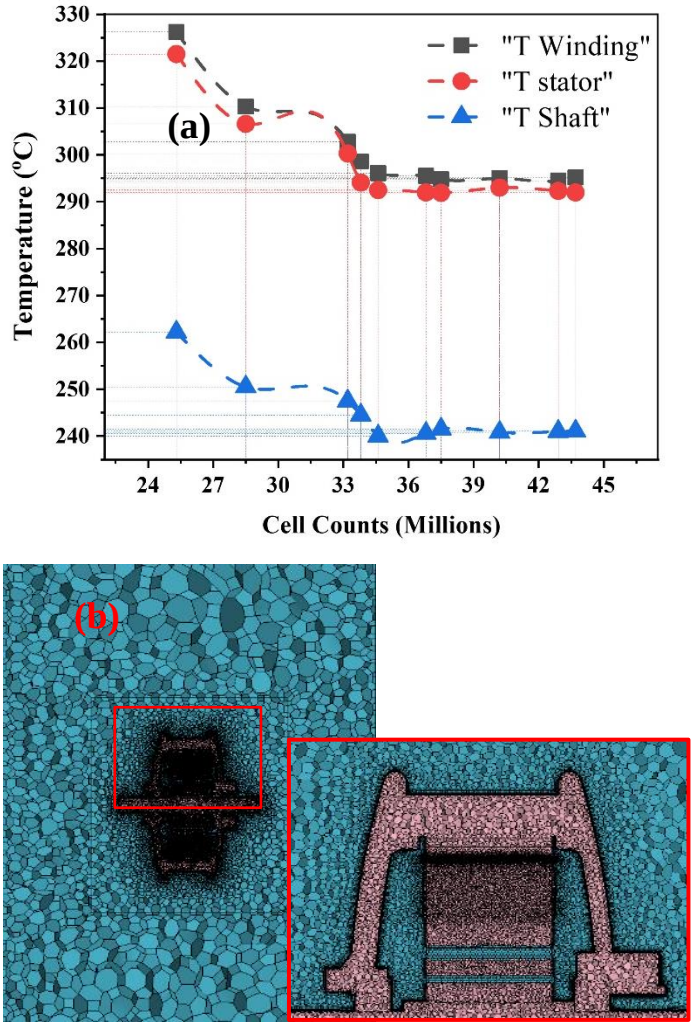

Figure 4. Shows the mesh independent study and meshing of the motor (a) Shows the variation of temperature on the motor components with increasing number of cells (b) Shows the meshing of the motor components and fluid domains.

The model described in this section is used to carry out a parametric study that is implemented in Taguchi's Design of Experiments (DOE).

Taguchi's Optimisation with Design Manager Study

The main aim of Taguchi's optimization study is to identify design parameters (optimum number) that have a huge effect on decreasing the temperature of the windings and increasing the heat transfer. Taguchi's process of optimization has three stages [27].

- System design – focuses on the design at a conceptual level, which involves creativity, innovation, and imagination.
- Parameter design – set the nominal values of various dimensions or design parameters for optimisation.

- Tolerance design – understanding the effect of various parameters on the required objective, resources might be concentrated on minimizing and managing variation in a selected few crucial dimension.

The introduction of design parameters such as air-vents/holes and both internal and external fins on the surface of the rotor could decreases the convection thermal resistance, and increases the local heat transfer coefficient, hence the effective heat transfer rate. Further, it could also increase the stator winding's heat transfer coefficient as a result of increasing local velocities and turbulence. The modifications to the rotor (air vents/channels and fins) are set as design parameters in the simulation setup, these design parameters are the factors in Taguchi's Design of Experiments analysis. Figure 5(a-b) shows the design modification with design parameters such as fins and air vents on the surface of the rotor.

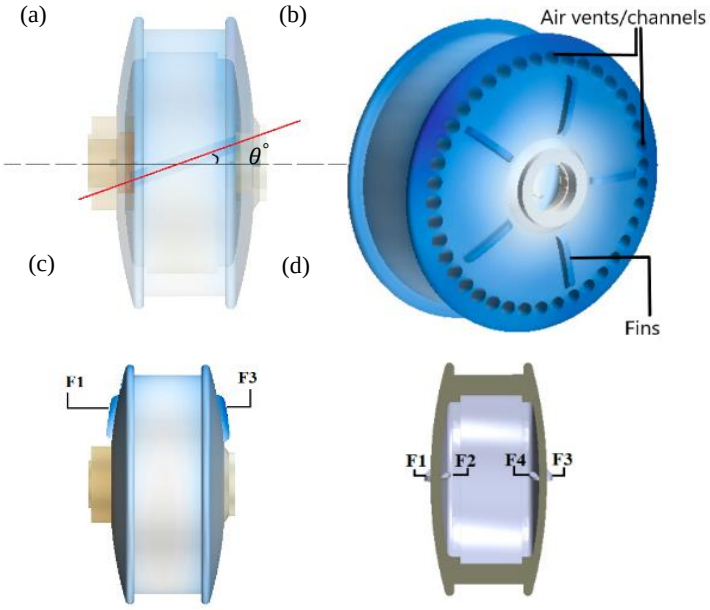

Figure 5. Shows the design parameters on the surface of the rotor (a) shows the rotor with air vents/channel inclination to motor axis (b) rotor with air vents and fins (c-d) Shows the fins on the rotor and rotor lids (F1-F4).

Table 3 is a list of the factors (design parameters), their tolerance range for variations that are possible on the rotor surface. All of these 6 parameters and their 5 levels of values resulted in 15625 design combinations and Taguchi's DOE reduced it to 25 design cases, which have run in the design manager study platform in StarCCM+ software. All these design cases are optimised for minimum winding temperature, minimum rotor heat flux for a Taguchi's situation 'smaller the better' and maximum heat transfer for a Taguchi's situation 'larger the better'.

Table 3. The design parameters and its tolerance range used in the design manager study

Parameters		θ˚	V1	F1	F2	F3	F4
Range		12-20	1-40	1-35	1-35	1-35	1-35
Levels	1	12	1	1	1	1	1
	2	14	10	5	5	5	5
	3	16	20	15	15	15	15
	4	18	30	25	25	25	25
	5	20	40	35	35	35	35

Where θ˚ -The inclination of air vent axis with the rotational axis of the motor, V1-Number of holes/air-vents on the rotor surface, F1-Number of Fins on the rotor outer surface, F2-Number of fins on the rotor internal surface., F3-Number of fins on the rotor-lid/rotor cover external surface, F4-Number of fins on rotor lid/rotor cover internal surface.

Result and discussion

The study of external aerodynamics is important to understand the fluid flow near the rear wheel motor region, especially when the research is mainly focusing on aerodynamic cooling or combined cooling. The rate of cooling of the motor depends on the available air at the rear end of the wheel.

External aerodynamics

External aerodynamic simulations have been performed for the scooter and a passenger. The velocity and pressure profile has been generated on various planes on the rear wheel of the scooter to evaluate the percentage of available air near rear wheel region. Only 80% of total air velocity (5.5m/s) is available at the rear wheel region. Figure 6 (a-b) shows the velocity profile at the rear wheel region of the scooter. The heat transfer coefficient of a surface is a function of fluid flow velocity, density, characteristic length, fluid viscosity and specific heat capacity [28]. So, the heat transfer from the rotor surface to the ambient air depends on the available air flow near the wheel region. To improve the heat transfer from the wheel surface, the local heat transfer coefficient can be increased by increasing the local velocity near the wheel region. The external aerodynamics analysis showed that the airflow velocity could be lower than the free stream velocity by 80% as shown in Figure 6(a-b). Air velocity lower than 80% (0.5m/s) of the available air flow around the wheel has been considered when simulating the wheel alone without the full geometry of the scooter.

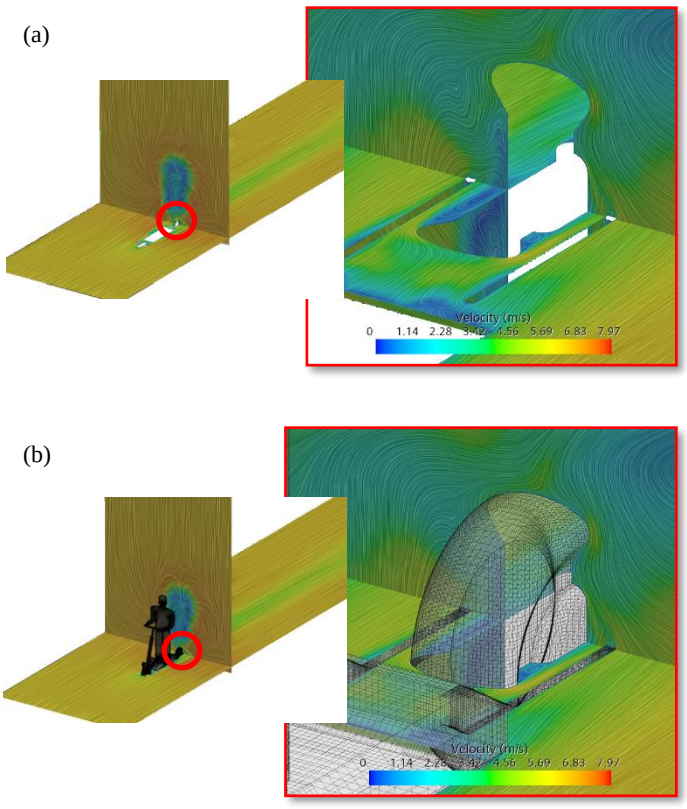

Figure 6. Shows the velocity profile for external aerodynamic simulation analysis. (a-b) velocity profile without scooter body and with scooter body respectively.

Local velocity near the wheel region can be increased by generating a pressure drop. Without the air holes and fins on the rotor surface the pressure between two sides of the wheel remained equal, Figure 7(a) shows the pressure distribution at rear wheel region. An increase in local velocity can be achieved by generating a pressure drop across the wheel using the fins and air-vents/holes around the rotor circumference Fins can be used to direct the fluid flow to the air holes or vents. Figure 7(b-c) shows the introduction of air hole/vents and fins on rotor surface and pressure drop between two surfaces of the rotor near air holes. In addition, such geometric modifications increase the effective heat transfer surface. However, a conjugate heat transfer analysis is relevant to determine the heat transfer path and thermal resistances at the interfaces to evaluate whether such modification could possibly increase the heat transfer or reduce thermal resistance.

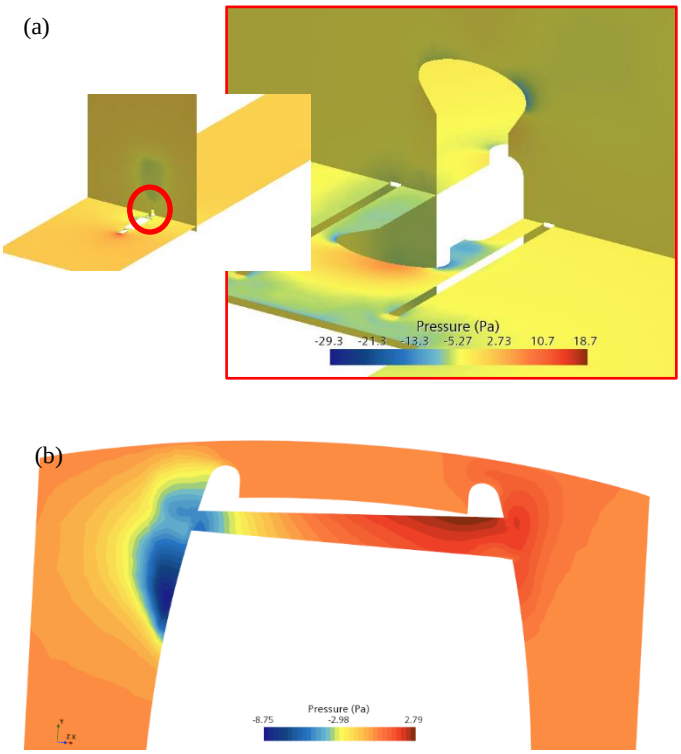

Figure 7. Shows the external pressure distribution for a scooter with passenger and rotor (a) pressure distribution at the rear wheel region without any design modifications (b) pressure drop between two sides of the wheel or rotor as a result of the design modifications air holes/vents and fins.

Conjugate heat transfer

The copper heat loss in the stator is the major loss in the PMBLDC motors [29]. Conjugate heat transfer analysis on wheel hub motor is carried out for steady state heat generation of 180W (*worst scenario of climbing an uphill of slope greater than 3° based on calculation from literature described in methodology session*) in the windings (*64% efficiency*) for a speed of 482rpm. At this operating condition, the temperature on the winding increased to 297°C. Figure 8(a) shows the temperature distribution in the solid domain and fluid domain. The components such as stator and shaft also reached a local higher temperature, 297°C and 267°C, respectively. Figure 8 (b) & (c) present the temperature distribution in the rotor and shaft component. The temperature on the windings are expanding beyond the thermal class of insulation materials available in the market [30].

The average temperature on the windings and stator remained almost same even though there is a radial temperature difference of 30°C on the stator. For the case of the shaft it is observed that there is an axial temperature difference of 50°C. On the rotor surface, the maximum temperature is observed near the shaft region and temperature gradient in the whole solid domain is only 4°C, which indicates that the rotor is at uniform temperature. Both the shaft and rotor have convection heat transfer boundaries, the temperature difference (ΔT) for the rotor and shaft with the ambient air (T=20°C) is 130°C and 96°C respectively. This temperature difference is the reason for the convection heat transfer at its boundaries. Due to the rotation of the wheel, the available airflow and tangential velocity reach its maximum at the periphery of the rotor. These temperature difference and tangential velocity

constitute a higher heat transfer rate across the rotor boundary than the shaft boundary. The narrow air gap (5mm) between the stator and rotor act as a thermal barrier and constitute for a temperature difference of 140°C. This high temperature difference for this narrow air gap is due to the Nusselt number (Nu) being approximately equal to 2 and the fluid flow is laminar. Figure 8 (d) presents the temperature distribution in the narrow airgap. Low Nu in the air gap indicates that the conduction dominates the heat transfer and low thermal conductivity of air result in low heat transfer and high temperature (140°C).

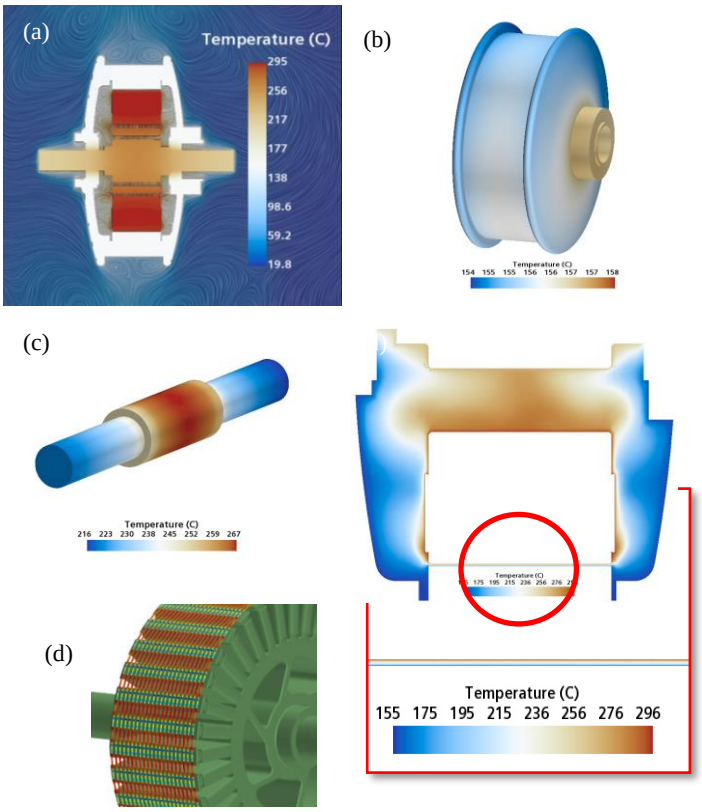

Figure 8. Shows the temperature distribution in wheel hub motor components for a steady state power loss of 180W in windings (a) temperature distribution on simulation domain at 482rpm (b) Shaft temperature at 482rpm (c) narrow air-gap the thermal barrier and zoomed view of thermal barrier (d) shows the air gap laminar fluid flow.

Figure 9(a-b) Shows the temperature dependency of each motor components with the speed of the motor. At low speed for a constant heat loss of 180W the maximum temperature on the winding could be as high as 490°C. The PMs, Sleeve and rotor average temperatures follow the same temperature profile with the speed of the rotor and the temperature difference is negligibly small. This is due to the geometric construction of the motor.

The conjugate heat transfer study is performed at various rotational speed (200rpm -1000rpm) and the average heat transfer coefficient for the outer rotor, air gap region, and stator has been calculated. Figure 8 shows the variation of heat transfer coefficient at the air gap between the rotor surface and stator surface with the speeds of the rotor. The stator air gap heat transfer coefficient is observed to be higher as compared to the outer rotor heat transfer coefficient, which enhances the internal heat transfer via convection to the outer rotor. With a higher air gap heat transfer coefficient higher heat transfer rate is expected for the internal air, 85% of the total heat generated in the stator winding is transferred to the internal air via convection and the rotor surface transfers 96.6% of the total heat to the ambient air. This difference in the heat transfer rate is due to the difference in temperature gradient in the internal air and ambient air. This shows that the temperature due to power loss and heat transfer coefficient do not show any correlation and the heat transfer coefficient only depends on the rotational speed, which indicates that the flow is dominated with viscous force rather than the buoyancy force due to density gradient.

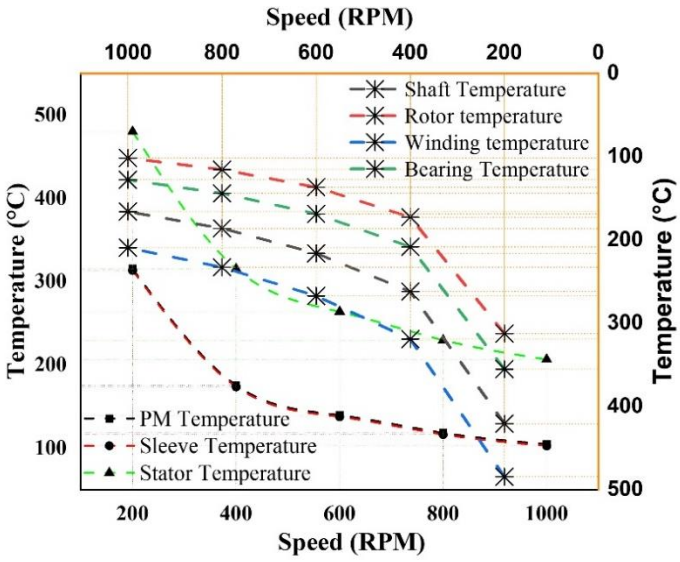

Figure 9. Shows the variation of the average temperature on stator and rotor components with speed of the motor.

To improve the heat transfer from the windings to the ambient air, it is important to understand the heat transfer path and interface thermal resistance. It is possible to either increase the heat transfer on a low thermal resistance path or a high thermal resistance path depending upon the design constraints and cooling requirement. Depending on the thermal sensitivity of the components, such as PMs and winding insulation, the appropriate cooling method can be introduced to ensure that the temperature on such components does not exceed the safe limit. The thermal limit of the insulation material varies with the commercially available class of the winding material, class105 to class240 [30]. PMs thermal limit varies from 120°C to 300°C depending upon the type of elements it possesses, Neodymium based PMs has the lowest thermal limit but more magnetic field intensity [31]. Accounting all these factors and the requirement of cooling windings and PMs, the thermal simulation analysis plays a vital role in determining the safe operation and also the performance enhancement of PMs based motors. Considering these requirements with the conjugate heat transfer thermal model, the convection-conduction heat transfer path (thermal path) and the thermal resistance at each interface has been developed and determined.

The heat transfer evaluation resulted in determining the maximum and minimum heat transfer path, the maximum heat transfer happens in the radial direction from the windings and stator to air gap and then to the PMs on the rotor. The result shows that approximately, 26.5% (47.8W) and 58.6% (105.63W) of total heat (100%, 180W) is transferred via

convection from the windings and stator to the air inside the motor respectively. Approximately, 73.8% (133.08W) of total heat is transferred to the stator via conduction of which 15.3% (27.7W) is conducted to the shaft. The maximum heat transfer is in the radial direction from the internal air to the PMs and then to the rotor and finally, to the ambient air, approximately 58.1% (104.57W) is transferred in the radial direction. Figure 11 shows the overall heat flow in the motor along the heat transfer path and the percentage heat transfer rate in each path.

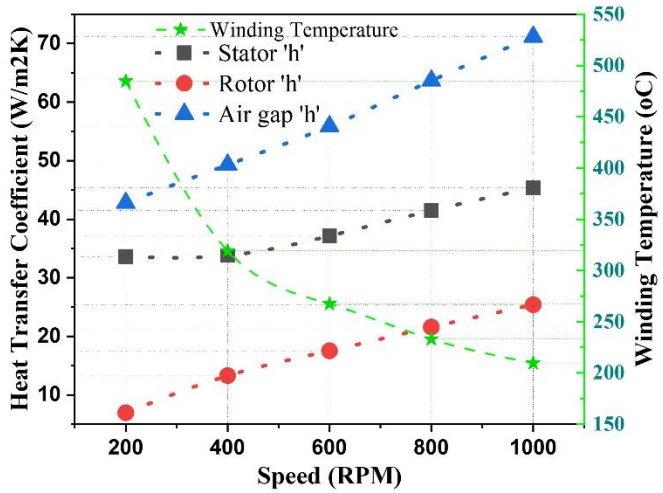

Figure 10. Shows the stator, rotor surface and air gap average heat transfer coefficient with speed of the rotor

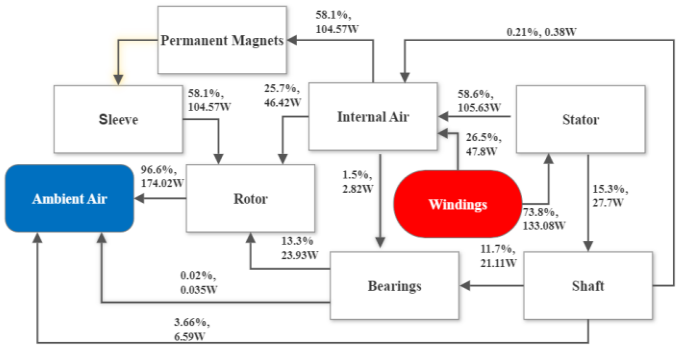

Figure 11. Shows the heat transfer path in the motor and the percentage of total heat transferred in each path.

All these thermal paths are associated with thermal resistance, reducing the thermal resistance further enhances the heat transfer across the boundary. For a boundary, the heat transfer rate across the boundaries and the temperature difference can give the thermal resistance value for that specific boundaries or interfaces. Thermal resistance at the boundaries is calculated as,

$$R_{th} = \frac{\Delta T}{Q} K/W$$

Where ΔT is the difference between the temperatures at both sides of the interface or boundary, Q – the heat transfer rate across the boundary

The interface thermal resistance for all the components in the motor is shown in Figure 12. The surface of the shaft has three heat transfer interfaces, with internal and external fluid and one with stator. The thermal resistance at shaft-internal air interface and shaft-stator interface is significantly higher, which is in the range of 31K/W-59K/W and 22.1K/W-62K/W, respectively when the speed of the rotor varies from 1000-200rpm. Whereas other components' thermal resistance are in the range of 0-3K/W. These high thermal resistance at the interfaces of the shaft are the major reason for the low heat transfer via conduction and convection from the shaft surface. When the speed of rotation increases 200rpm to 400rpm the thermal resistance decreases significantly and thereafter the change in thermal resistance decreases as the speed increases. This indicates that after a certain speed limit, the slope of the thermal resistance curve approaches zero. Figure 12 shows the thermal resistance of the components at the solid-solid and solid-fluid interfaces. R1-R9 indicate the interface thermal resistances, Table 4, list out the interfaces and corresponding thermal resistance representation.

Table 4. The thermal resistance representation to interfaces.

Thermal resistance	Interfaces
R1	Shaft – Internal air interface
R2	Shaft – ambient air interface
R3	Shaft – Stator interface
R4	Winding – internal air interface
R5	Winding – Stator interface
R6	Stator – internal air interface
R7	Rotor – Internal air interface
R8	Rotor ambient air - interface
R9	PMs – Internal air interface

Decreasing thermal resistance in a required heat transfer path enhances the heat transfer rate. Rotor surface modification is a potential approach to enhance the heat transfer rate. In the earlier discussion, the introduction of fins and air vents to the rotor surface has generated a pressure drop between the two sides of the wheel and increased the effective surface area. As a result, this could reduce the thermal resistance at the interfaces. Considering this few design modifications (fins and air vents) are introduced to the surface of the rotor to carry out design manager study and an optimization approach to identity the most significant design parameters to enhance the heat transfer.

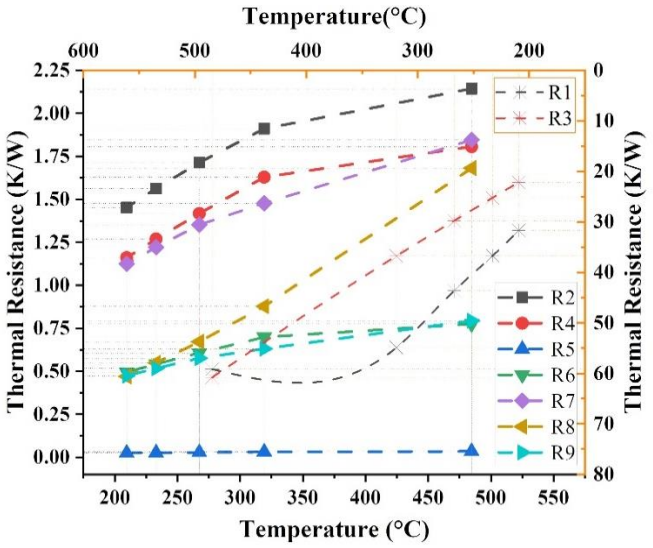

Figure 12. Shows the thermal resistance at each interface of the motor components

Taguchi's Optimization

Taguchi's DOE suggested 25 design cases and each design is run on design manager study in StarCCM+. Each design is considered as an experiment and carried out design of experiment analysis in Minitab. The result shows that, the minimum temperature is observed for the design with maximum number of air vents and external rotor fins. The variance delta in the mean response of temperature is above 20°C due to the presence of design parameters air-vents and external fins. Which shows that the number of air vents or holes and fins on external surface of rotor and rotor lid respectively has greater effect on decreasing the temperature on the winding. The minimum temperature observed in the design studies is 238.3°C. Table 5 and Table 5a shows the mean response for the winding temperature on rotor surface. Among all the parameters the rank 1, 2 and 3 has the most significant effect on decreasing the maximum temperature in the winding. This indicate that the parameters such as the number of air-vents, fins on rotor lid and number of fins on rotor external surface has the greatest effect on decreasing the winding temperature spike.

Table 5. Shows the design manager parameters mean response table for on winding temperature

Levels		1	2	3	4	5	Delta	Rank
θ°	Levels	12	14	16	18	20		
	T (°C)	250.4	244.3	243.7	251.9	244.8	8.2	6
V1	Levels	1	10	20	30	40		
	T (°C)	262.6	247.5	244.9	241.8	238.3	**24.3**	**2**

Table 5a. Shows the design manager parameters mean response table for on winding temperature

	Levels	1	5	15	25	35	Delta	Rank
Number of fins	F1 T (°C)	259.8	249.8	239.1	247.9	238.5	**21.3**	**3**
	F2 T (°C)	261.1	258.7	240.5	236.5	238.2	**24.6**	**1**
	F3 T (°C)	248.8	247.0	243.6	242.1	253.6	11.5	10.6
	F4 T (°C)	247.2	245.9	254.0	244.6	243.4	4	5

As the effective heat transfer area increases with the introduction of design parameters the heat flux across the rotor surface decreases for a constant heat load and speed. Table 6 and Table 6a shows the mean response of heat flux on the rotor surface. The parameters which can give maximum delta variation have the lowest heat flux value, which indicate that these parameters have greatest effect in decreasing heat flux by increasing the surface area. Such parameters are ranked 1, 2, and 3 in the mean response table.

From the mean plot it can be seen that with the increase in the number of air vents both the winding temperature and heat flux decreases for a constant heat load of 180W at a constant speed of 482rpm. Figure 13 and Figure 14 present the main effect plot for means of winding temperature and rotor surface heat flux respectively.

Table 6. Shows the design manager parameters mean response table for rotor boundary heat flux

Levels		1	2	3	4	5	Delta	Rank
θ°	Levels	12	14	16	18	20		
	W/m²	1473	1435	1424	1448	1414	59	4
V1	Levels	1	10	20	30	40		
	W/m²	1886	1602	1387	1224	1095	791	1

Table 6a. Shows the design manager parameters mean response table for rotor boundary heat flux.

	Levels	1	5	15	25	35	Delta	Rank
Number of fins	F1 W/m²	1484	1477	1420	1438	1357	109	3
	F2 W/m²	1497	1492	1439	1394	1373	124	2
	F3 W/m²	1445	1430	1420	1435	1463	43	5
	F4 W/m²	1450	1423	1455	1419	1447	36	6

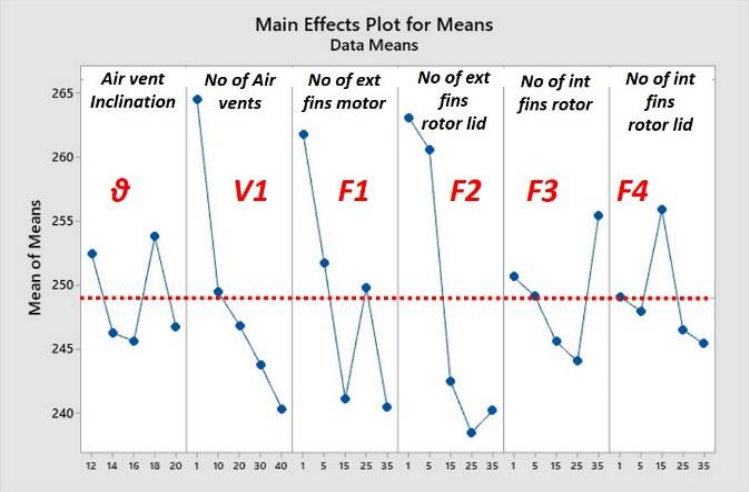

Figure 13. Shows the mean response of the winding temperature with design parameters.

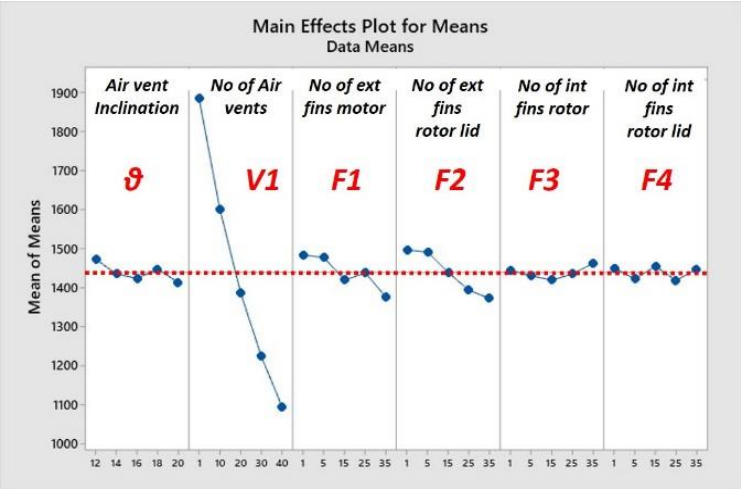

Figure 14. Shows the of the winding temperature and rotor heat flux with the design parameters

From Taguchi's DOE study, it has been observed that the lowest temperature on the winding is observed for the designs with design parameter values θ°-12, V1-40, F1-35, F2-35, F3-35, F4-35 and θ°-20, V1-40, F1-25, F2-5, F3-15, F4-1 as 229℃ and 232℃ respectively. The optimized design parameters are θ°-20, V1-40, F1-35, F2-1, F3-35, F4-1 and with this the temperature on the windings has been reduced to 228℃. With the optimized design the maximum temperature on the winding has been decreased by 68℃, Figure 15.

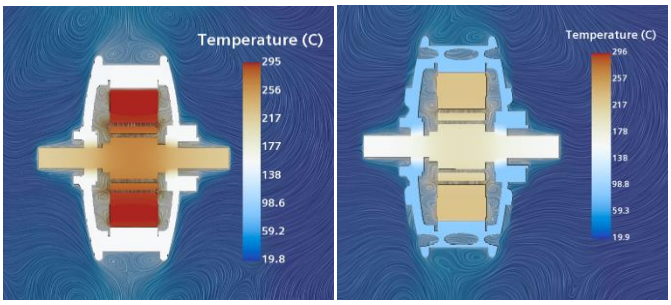

Figure 15. Shows the comparison of the temperature distribution on the motor between the baseline result and optimized result.

Conclusion

A scooter with a standing passenger and a BLDC motor CFD simulation has been carried out in StarCCM+. Two separate CFD simulations has been carried out, firstly to investigate the external aerodynamics and secondly to investigate the motor conjugate heat transfer. Fluid flow velocity and pressure near the rear wheel of the scooter has been investigated. No pressure difference has been observed between the two sides of the rear wheel. Fins and air vents are introduced to the rotor surface to generate local velocity. The introduced design resulted in a pressure drop of 7Pa between two sides of the wheel. Then a CFD-based conjugate heat transfer on a wheel hub motor has been numerically evaluated and determined the thermal path and thermal resistances at the interfaces.

Both internal and external fluid region is considered to determine the heat transfer path and thermal resistance. Maximum heat of approximately 96% of the total heat is transferred to the ambient air through the rotor, and 58% of the total heat is transferred along the radial direction to the permanent magnet in the rotor. Thermal resistance plays an important role in deciding the heat transfer path, the shaft interfaces has a higher thermal resistance compared to other component's interfaces in the motor which results in low heat transfer through the shaft via conduction. The thermal path and pressure drop across the wheel with fins and air vents lead to the ways of introducing design parameters to enhance the heat transfer. With the design parameters, Taguchi's optimization has been carried out and found that the air vents/holes and external fins on the rotor have the greatest effect in reducing the winding temperature among all the design parameters. With the introduction of air vents and external fins the winding temperature has reduced by 68℃. These efficient design parameters also have a greater effect in enhancing the heat flux by increasing the effective heat transfer area on the rotor surface for a constant heat load of 180W and 482rpm.

Recommendations

Further modification of the air vents and external fins to increase the pressure drop between two sides of the rotor can enhance the heat transfer. Advanced ad-joint shape optimization of the fins and air-vents can further improve the heat transfer and reduce the temperature spike in the winding. Thus, it would improve the performance and life of the wheel hub motor, which would be considered in our future research study. Testing and validating the numerical results is required before progressing or applying this cooling approach to wheel hub motors. This aerodynamic cooling approach can be used in combination with other cooling methods and can be scaled up to apply in any type of traction motor.

References

[1] O. Korzilius, O. Borsboom, T. Hofman, and M. Salazar, 'Optimal design of electric micromobility vehicles', in *2021 IEEE International Intelligent Transportation Systems Conference (ITSC)*, 2021, pp. 1677–1684.

[2] D. Hirst, 'Regulating electric scooters (E-scooters)', *House of Commons Library, London. Briefing Paper*, vol. 8958, no. 10, 2021.

[3] P. Posirisuk, C. Baker, and M. Ghajari, 'Computational prediction of head-ground impact kinematics in e-scooter falls', *Accident Analysis & Prevention*, vol. 167, p. 106567, 2022.

[4] A. D. Bozzi and A. Aguilera, 'Shared E-scooters: a review of uses, health and environmental impacts, and policy implications of a new micro-mobility service', *Sustainability*, vol. 13, no. 16, p. 8676, 2021.

[5] D. M. S. Bodansky *et al.*, 'Legalisation of e-scooters in the UK: the injury rate and pattern is similar to those of bicycles in an inner city metropolitan area', *Public health*, vol. 206, pp. 15–19, 2022.

[6] M. Barker, T. Pepper, R. Dua, and K. Fan, 'Electric scooters: convenient transport or ED headache?', *British journal of oral and maxillofacial surgery*, vol. 60, no. 2, pp. 199–200, 2022.

[7] J. Vanus and P. Bilik, 'Research on Micro-Mobility with a Focus on Electric Scooters within Smart Cities', *World Electric Vehicle Journal*, vol. 13, no. 10, p. 176, 2022.

[8] B. Şengül and H. Mostofi, 'Impacts of E-Micromobility on the sustainability of urban transportation—a systematic review', *Applied Sciences*, vol. 11, no. 13, p. 5851, 2021.

[9] B. Gombert, R. Fischer, and W. Heinrich, 'Wheel-hub motors. Criteria of construction and vehicle integration; Elektrische Radnabenmotoren. Konstruktionskriterien und Fahrzeugintegration', 2010.

[10] C. Wohlers, P. Juris, S. Kabelac, and B. Ponick, 'Design and direct liquid cooling of tooth-coil windings', *Electrical Engineering*, vol. 100, no. 4, pp. 2299–2308, 2018.

[11] Z. Huang, F. Marquez, M. Alakula, and J. Yuan, 'Characterization and application of forced cooling channels for traction motors in HEVs', in *2012 XXth International Conference on Electrical Machines*, 2012, pp. 1212–1218.

[12] M. Polikarpova, P. Ponomarev, P. Röyttä, S. Semken, Y. Alexandrova, and J. Pyrhönen, 'Direct liquid cooling for an outer-rotor direct-drive permanent-magnet synchronous generator for wind farm applications', *IET Electric Power Applications*, vol. 9, no. 8, pp. 523–532, 2015.

[13] S. A. Semidey and J. R. Mayor, 'Experimentation of an electric machine technology demonstrator incorporating direct winding heat exchangers', *IEEE Transactions on Industrial Electronics*, vol. 61, no. 10, pp. 5771–5778, 2014.

[14] M. Schiefer and M. Doppelbauer, 'Indirect slot cooling for high-power-density machines with concentrated winding', in *2015 IEEE International Electric Machines & Drives Conference (IEMDC)*, 2015, pp. 1820–1825.

[15] M. H. Park and S. C. Kim, 'Thermal characteristics and effects of oil spray cooling on in-wheel motors in electric vehicles', *Applied Thermal Engineering*, vol. 152, pp. 582–593, 2019.

[16] K.-H. Lee, H.-R. Cha, and Y.-B. Kim, 'Development of an interior permanent magnet motor through rotor cooling for electric vehicles', *Applied Thermal Engineering*, vol. 95, pp. 348–356, 2016.

[17] M. Fasil, D. Plesner, J. H. Walther, N. Mijatovic, J. Holbøll, and B. B. Jensen, 'Numerical and Experimental Investigation of Heat Flow in Permanent Magnet Brushless DC Hub Motor', *SAE International Journal of Alternative Powertrains*, vol. 4, no. 1, pp. 46–57, 2015.

[18] S. Nategh *et al.*, 'A review on different aspects of traction motor design for railway applications', *IEEE Transactions on Industry Applications*, vol. 56, no. 3, pp. 2148–2157, 2020.

[19] M. L. Hosain, R. B. Fdhila, and K. Rönnberg, 'Air-gap flow and thermal analysis of rotating machines using CFD', *Energy Procedia*, vol. 105, pp. 5153–5159, 2017.

[20] D. A. Howey, P. R. Childs, and A. S. Holmes, 'Air-gap convection in rotating electrical machines', *IEEE transactions on industrial electronics*, vol. 59, no. 3, pp. 1367–1375, 2010.

[21] E. Gundabattini, R. Kuppan, D. G. Solomon, A. Kalam, D. P. Kothari, and R. A. Bakar, 'A review on methods of finding losses and cooling methods to increase efficiency of electric machines', *Ain Shams Engineering Journal*, 2020.

[22] S. R. Allmaras and F. T. Johnson, 'Modifications and clarifications for the implementation of the Spalart-Allmaras turbulence model', in *Seventh international conference on computational fluid dynamics (ICCFD7)*, 2012, vol. 1902.

[23] D. W. Zingg and P. Godin, 'A perspective on turbulence models for aerodynamic flows', *International journal of computational fluid dynamics*, vol. 23, no. 4, pp. 327–335, 2009.

[24] R. Wrobel, P. H. Mellor, N. McNeill, and D. A. Staton, 'Thermal performance of an open-slot modular-wound machine with external rotor', *IEEE Transactions on Energy Conversion*, vol. 25, no. 2, pp. 403–411, 2010.

[25] M. S. Khande, M. A. S. Patil, M. G. C. Andhale, and M. R. S. Shirsat, 'Design and Development of Electric scooter', *Energy*, vol. 40, no. 60, p. 100, 2020.

[26] B.-M. Song, K.-C. Chang, and J.-Y. Choi, 'Design of an outer-rotor-type permanent magnet motor for electric scooter propulsion systems', in *The 2010 International Power Electronics Conference-ECCE ASIA-*, 2010, pp. 2763–2742.

[27] S. K. Karna and R. Sahai, 'An overview on Taguchi method', *International journal of engineering and mathematical sciences*, vol. 1, no. 1, pp. 1–7, 2012.

[28] A. Carriero, M. Locatelli, K. Ramakrishnan, G. Mastinu, and M. Gobbi, 'A review of the state of the art of electric traction motors cooling techniques', 2018.

[29] B. Singh and S. Singh, 'State of the art on permanent magnet brushless DC motor drives', *journal of power electronics*, vol. 9, no. 1, pp. 1–17, 2009.

[30] Y. Yang *et al.*, 'Thermal management of electric machines', *IET Electrical Systems in Transportation*, vol. 7, no. 2, pp. 104–116, 2017.

[31] J. M. D. Coey, ‘Permanent magnet applications’, *Journal of Magnetism and Magnetic Materials*, vol. 248, no. 3, pp. 441–456, 2002.

Contact information

Arun Mambazhasseri Divakaran
Coventry University, United Kingdom
Email: mambazhasa@uni.coventry.ac.uk

Dr. Evangelos Gkanas
Email: evangelos.gkanas@coventry.ac.uk

Acknowledgement

The authors wish to acknowledge GCRF (Global Challenge Research Fund) for supporting this work and Mubea Ltd for providing technical support and the CAD drawings of the motor.

Response to Reviewers

Response to Reviewer 1 #: 312719

This paper performs basic heat transfer study to an electric motor which is well known of convection through air gaps and conduction through physical contact. When author tried to quantify all heat transfer percentage in each of the means, it will be helpful and benefit readers with following questions clarified and updates:

Comment 1

1. When top speed is set as 18kph (5m/s), how was the internal air velocity assumed to be 0.5m/s which listed at Fig.3 (b) then Page 4?

Responds to comment 1:

The authors wish to thank Reviewer 1 for mentioning this and give us the opportunity to explain this in more detail.

Two types of numerical analysis have been carried out in this research work. Firstly, for the external aerodynamics with the scooter and the passenger standing on it to understand the external aerodynamic fluid flow at the rear wheel side of the scooter. Due to the presence of the scooter's frontal body, rear tire and passenger body, the availability of air at the rear wheel region is low, approximately only 20% (~1m/s) of the fluid velocity is available at the rear wheel near region. The presence of the tire on wheel or any other object further blocks the airflow. Considering this as the worst scenario we have assumed velocity as 0.5m/s for a separate conjugate heat transfer simulation analysis.

Comment 2

2. At Page 2, it says simulation used 4.75million cells, while Fig 4(a) shows variation of cells starting from 24 Million. Given the temperature result is lower with more cells, what did model build in the end?

Response to comment 2:

This is a solid comment and we wish to expand and explain in more detail,

We have presented two simulation scenarios one for external aerodynamics and the other for conjugate heat transfer analysis. For external aerodynamic analysis, the simulation domain considers only the fluid domain, and the number total number of cells is 4.75 million. The motor-only simulation (conjugate heat transfer) analysis consisting of two fluid domains (external and internal) and a solid domain have significantly increased the number of cells to 34.6 million cells when the mesh converges to capture the small feature's effects. A standard mesh-independent study has been carried out to ensure that the temperature is independent of the mesh size.

Comment 3

3. Page 5, Table 3 - would you please list the details for 6 design parameters? V1 or F1 etc, what does it stand for?

Response to comment 3:

We have added these missing details to Table 3 to make the parameters clear and the Table 3 has been updated as follows in the manuscript.

Table 1. The design parameters and its tolerance range used in the design manager study

Parameters		θ°	V1	F1	F2	F3	F4
Range		12-20	1-40	1-35	1-35	1-35	1-35
Levels	1	12	1	1	1	1	1
	2	14	10	5	5	5	5
	3	16	20	15	15	15	15
	4	18	30	25	25	25	25
	5	20	40	35	35	35	35

Please see the details of 6 design parameters, θ°, V1 and F1 to F4, which are included just below Table 3 in the manuscript.

Where θ° -The inclination of air vent axis with the rotational axis of the motor, V1-Number of holes/air-vents on the rotor surface, F1-Number of Fins on the rotor outer surface, F2-Number of fins on the rotor internal surface, F3-Number of fins on the rotor-lid/rotor cover external surface, F4-Number of fins on rotor lid/rotor cover internal surface.

Additionally, Figure 5 has been updated with Clear figures showing the design parameters and are added to the manuscript as shown below. All these updates and modifications generate clarity and better understanding for the readers, once again thank you for the comment.

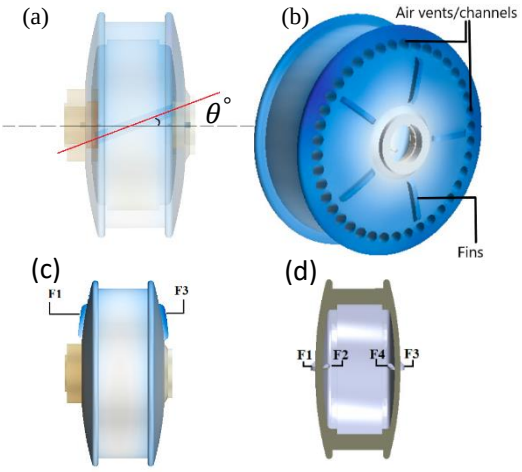

Figure 1. Shows the design parameters on the surface of the rotor (a) shows the rotor with air vents/channel inclination to motor axis (b) rotor with air vents and fins (c-d) Shows the fins on the rotor and rotor lids (F1-F4).

Comment 4

4. At Table 3, if each parameter has 5 levels, why the value has much bigger range? such as V1's value is from 1 to 40, what is 5 level detail?

Response to comment 4

The design parameters V1 and F1 to F4 has wide range of values that is 1-40 and 1-35 respectively. These values shows the lower and upper limit of the design parameter values, these are set based on the least and most possible number of design parameter on the motor design geometry. Each of these parameters has 5 levels and these 5 levels have been added to the Table 3 and included in the manuscript. The modified Table 3 has been shown below.

Table 2. The design parameters and its tolerance range used in the design manager study with 5 levels

Parameters		θ°	V1	F1	F2	F3	F4
Range		12-20	1-40	1-35	1-35	1-35	1-35
Levels	1	12	1	1	1	1	1
	2	14	10	5	5	5	5
	3	16	20	15	15	15	15
	4	18	30	25	25	25	25
	5	20	40	35	35	35	35

Where θ° -The inclination of air vent axis with the rotational axis of the motor, V1-Number of holes/air-vents on the rotor surface, F1-Number of Fins on the rotor outer surface, F2-Number of fins on the rotor internal surface, F3-Number of fins on the rotor-lid/rotor cover external surface, F4-Number of fins on rotor lid/rotor cover internal surface.

Comment 5

5. Page 6, if the high speed is limited and max rotation is 492rpm, when simulation expanded to 200-1000rpm, do you still assume 180w as maximum heat transfer? Typcially when rotor spins higher speed, the heat will go up too, thus Fig. 9 & 10 temperature prediction with higher speed won't be true.

Response to comment 5

The authors wish to thank Reviewer 1 for highlighting this.

The authors agree that when the motor spins at a higher speed with a constant load the heat generation will increase as the power increases and hence the temperature. But in this work, we have assumed a constant heat generation of 180W (as explained on the manuscript) for all the speed conditions due to the lack of valid data on how much heat is generated when the speed increases to 1000rpm, as the validation has not been done yet. This would be considered in our future work which we have mentioned in the conclusion section. The authors appreciate that under such drive conditions, the results might be slightly different however we are confident that the model can describe up to a certain point the actual behaviour of the motor.

Comment 6

6. Page 8, Table 5, would you please list the design level used to get Table 5's result? That will be the helping information for reader to know how design parameters were set to get the result, then adding a comparison of using optimized design parameters of V1, F1, F2, how much is the motor temperature changed or much below the limit

Response to comment 6

The design levels of each parameter used in Taguchi's DOE method are included to Table 5 and Table 6, which will help the readers to know more about the design parameters and its effect on temperature and heat flux respectively. These tables have been included in the manuscript.

Table 3. Shows the design manager parameters mean response table for on winding temperature

Levels		1	2	3	4	5	Delta	Rank
θ°	Levels	12	14	16	18	20		
	T (°C)	250.4	244.3	243.7	251.9	244.8	8.2	6
V1	Levels	1	10	20	30	40		
	T (°C)	262.6	247.5	244.9	241.8	238.3	**24.3**	**2**

Table 4a. Shows the design manager parameters mean response table for on winding temperature

	Levels	1	5	15	25	35	Delta	Rank
Number of fins	F1 T (°C)	259.8	249.8	239.1	247.9	238.5	**21.3**	**3**
	F2 T (°C)	261.1	258.7	240.5	236.5	238.2	**24.6**	**1**
	F3 T (°C)	248.8	247.0	243.6	242.1	253.6	11.5	10.6
	F4 T (°C)	247.2	245.9	254.0	244.6	243.4	4	5

Table 5. Shows the design manager parameters mean response table for rotor boundary heat flux.

Levels		1	2	3	4	5	Delta	Rank
θ°	Levels	12	14	16	18	20		
	W/m^2	1473	1435	1424	1448	1414	59	4
V1	Levels	1	10	20	30	40		
	W/m^2	1886	1602	1387	1224	1095	791	1

Table 6a. Shows the design manager parameters mean response table for rotor boundary heat flux.

	Levels	1	5	15	25	35	Delta	Rank
Number of fins	F1 W/m^2	1484	1477	1420	1438	1357	109	3
	F2 W/m^2	1497	1492	1439	1394	1373	124	2
	F3 W/m^2	1445	1430	1420	1435	1463	43	5
	F4 W/m^2	1450	1423	1455	1419	1447	36	6

Taguchi's DOE method study suggests 25 design cases, out of these design cases the lowest temperature has been observed for the design parameter values θ° -12, V1 – 40, F1 – 35, F2- 35, F3-35, F4- 35 and θ° - 20, V1 – 40, F1 – 25, F2- 5, F3-15, F4- 1, the lowest temperature is 229°C and 232°C respectively. Taguchi's DOE study also resulted in the most effective parameters on temperature reduction. The optimized design parameters are θ° - 20, V1 – 40, F1 – 35, F2- 1, F3-35, F4 – 1. F2 and F4 are the fins on the inner side of the rotor and rotor cover/lid which has least effect on decreasing temperature. With the optimized design parameters the temperature has reduced to 228°C and the

result has been compared with the baseline simulation result and added to figure 15 (shown below) in the manuscript.

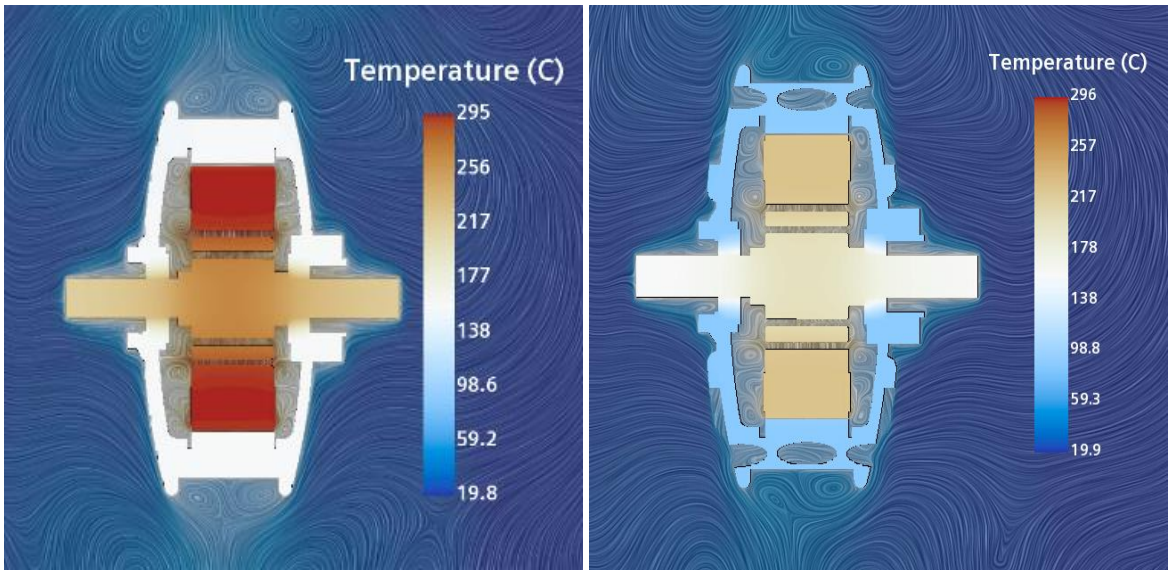

Figure 2. Shows the comparison of the temperature distribution on the motor between the baseline result and optimized result.

Response to Reviewer 2 #: 312721

This paper provides good overview of CFD analysis for a wheel hub motor for micro-mobility.

Comment 1

- It's nice to see a clear mesh sensitivity study, which is often left out of papers. It's unclear however what mesh size was used. In the text it says 4.75 million but in the study it appears to be much larger. Please make this more clear.

Response to comment 1

The authors wish to thank Reviewer 2 for giving us the opportunity to explain this in more detail.

The simulation study has two scenarios, firstly the external aerodynamics and secondly the conjugate heat transfer analysis for the motor. In the first simulation analysis, the fluid domain constituted 4.75 million cells and secondly, in the conjugate heat transfer analysis the simulation domain consisting of fluid and solid domains constituted 34.6 million cells. Both the simulation analysis are separate and the suggested changes have been made in the manuscript for better clarity

Comment 2

- There are some minor grammatical clean up items:
    - On page 2: ..the airflow distribution around the rotating when."
    - Page 4, "here in this study, A scooter…"
    - On page 8 I found the abbreviation "no." confusing. I would suggest just writing it out.

Response to comment 2

The suggested changed have been added in the manuscript

Comment 3

- The study would be greatly strengthened by validation results. Has an effort been made to validate the results?

Response to comment 3

This is indeed a very solid comment, and we wish to explain in detail.

Yes, we agree with your suggestion on validating the results. We are setting up the experimental arrangements to validate the results, almost 80% of the test rig has been completed. Now, introducing the controls and data acquisition systems to drive and collect data respectively. The experimental work will provide information about the amount of energy to be dissipated at various operation speeds. In this study this value was kept constant at 180W with the aim to understand the effect of various design parameters and which parameter has more influence on the heat transfer process.

We are setting up an experimental test rig to determine the heat loss at different drive conditions and also to validate the numerical results, which we believe would be possible in the near future.

Comment 4

- Figure 14 is low resolution and hard to read in a printout. Please improve the resolution.

Response to comment 4

We thank you for pointing out the pixelated figures in the manuscript, we have increased the resolution of the figures 14 and 15 and added to the manuscript.

Figure 3. Shows the mean response of the winding temperature with design parameters.

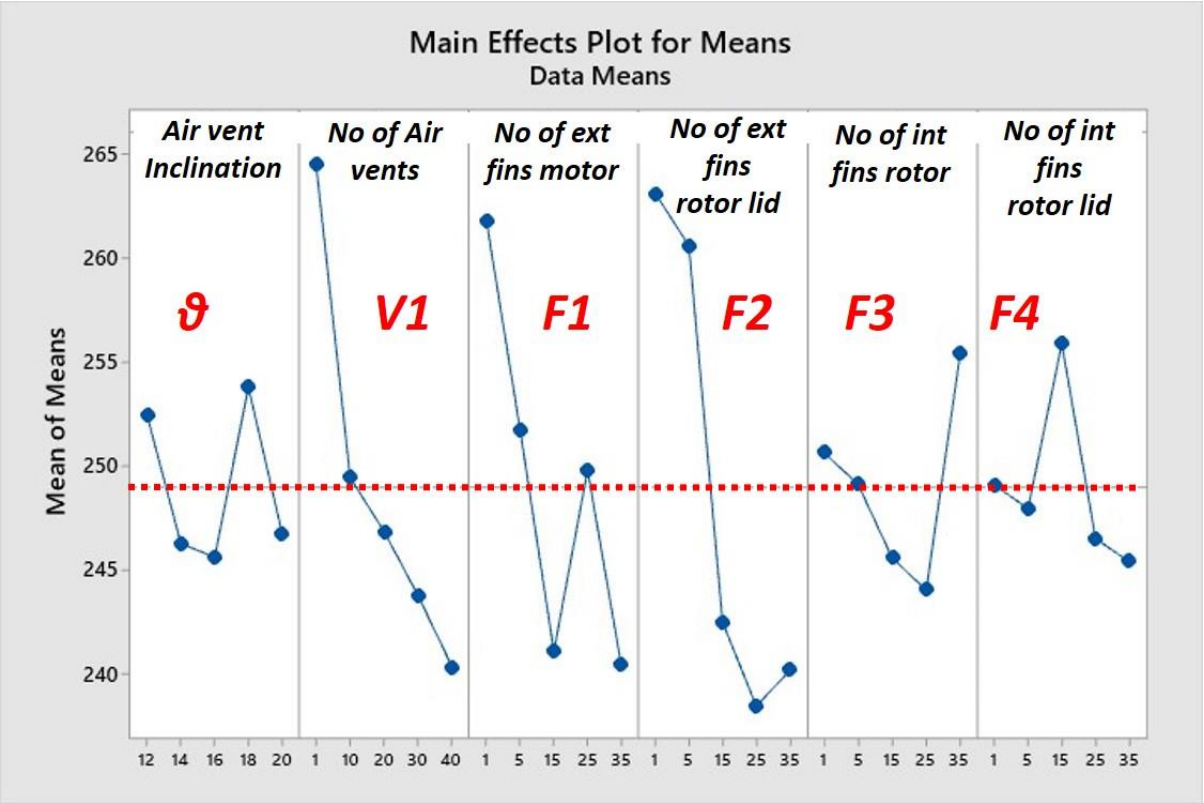

Figure 4. Shows the of the winding temperature and rotor heat flux with the design parameters

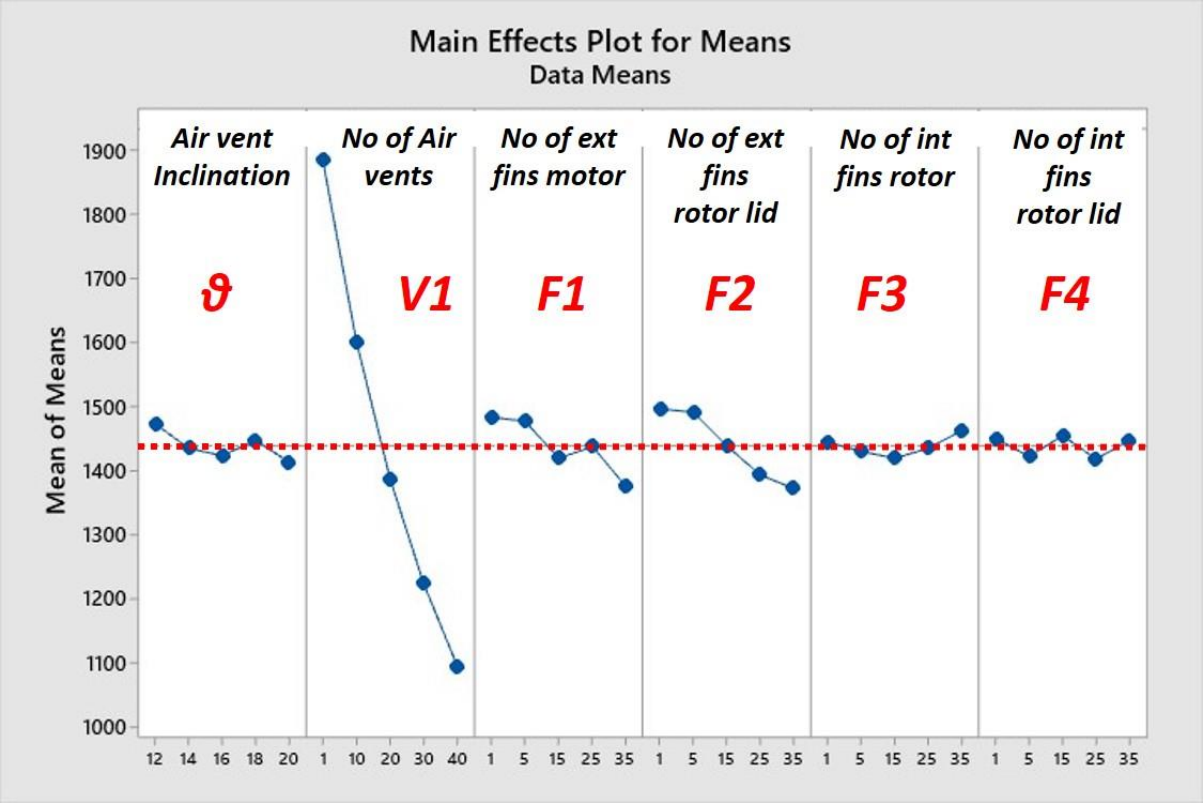

Comment 5

- Ad-joint optimization is mentioned a few times, but it is unclear if this method was used or is proposed for future work.

Response to comment 5

Adjoint optimization is out of the scope this research work and is a proposed optimization technique for the future works. (We haven't done any adjoint optimization in this study and we have removed these terms from the manuscript).